ISSN (Print) 1226-1750
ISSN (Online) 2233-6656
Journal of Magnetics 23(3), 399-404 (2018) https://doi.org/10.4283/JMAG.2018.23.3.399

Investigation on Texture, Magnetic Properties and Inhomogeneities of Hot Deformed Nd–Fe–B Magnet

Hongjian Li, Qiong Wu, Ming Yue*, Xiaochang Xu, Yuqing Li, Jingming Liang, Wang Xi, and Jiuxing Zhang

College of Materials Science and Engineering, Beijing University of Technology, Beijing 100124, China

(Received 2 May 2018, Received in final form 26 June 2018, Accepted 26 June 2018)

The anisotropic hot deformed nanocyrstalline Nd–Fe–B magnet was prepared by spark plasma sintering technique using MQU-F powders. The location dependence along radial direction on the magnetic properties, microstructure and crystal alignment of the hot deformed magnet have been investigated. The inhomogeneity of the magnetic performance along radial direction was revealed with a vibrating sample magnetometer (VSM). The crystal structure and microstructure were characterized by X-ray diffractometry (XRD) and scanning electron microscopy (SEM), respectively. In addition, quantitative texture analysis was carried out based on the electron backscattered diffraction technique (EBSD). The experimental results reveal that the coordination of grain size and orientation of Nd–Fe–B grains leads to the inhomogeneities of magnetic performance.

Keywords : Hot deformation, electron backscattered diffraction, crystallographic alignment, inhomogeneity

1. Introduction

The hot deformed Nd–Fe–B permanent magnets have drawn widely attention due to their high magnetic performance [1-6]. It is important to understand the relevance between the local magnetic properties and the local orientation texture features in hot deformed Nd–Fe–B magnets. Detailed investigation have revealed that its magnetic performance was inhomogeneous along axial direction which are parallel with the press direction [7, 8]. However, to the best of our knowledge, the systematic investigations on the inhomogeneities of the magnetic performance in hot deformed Nd–Fe–B bulk permanent magnet along the radial direction are insufficient.

Spark Plasma Sintering (SPS) is known as one of the novel sintering techniques. An important advantage of SPS is high sintering speed, which can effectively restrain the grain growth and allows the preparation of high-density fine crystalline materials [9-12]. In recent years, SPS has been widely applied to prepare bulk nanocrystalline Nd–Fe–B magnets [13, 14]. In spite of similar raw materials and processing conditions, a remarkable discrepancy in magnetic properties has been observed among different researchers, which suggests that the investigation on the relation between microstructure and magnetic properties of hot deformed Nd–Fe–B magnets prepared by SPS is still necessary.

In this paper, the relationship between magnetic properties and inhomogeneities of orientation texture in the different locations along radial direction of the hot deformed Nd–Fe–B magnet has been investigated. Hot deformed Nd–Fe–B bulk magnets were prepared by SPS method. The inhomogeneity of the magnetic performance along the radial direction was first revealed via a vibrating sample magnetometer (VSM). The morphology and microstructures in the different locations along radial direction were then examined to further reveal the origins of radial inhomogeneity of magnetic performance. In addition, more detailed information of the crystallographic texture evolution along radial direction was provided by use a powerful tool, electron backscatter diffraction (EBSD) [15-18].

2. Experiments

Commercial Nd–Fe–B magnetic powders (MQU-F) were used as initial materials. The magnetic powders were poured into a tungsten carbide (WC) mold and fast

*Corresponding author: Tel: 67391760
Fax: 67391760, e-mail: yueming@bjut.edu.cn

consolidated into columnar samples by using the SPS method. The temperature and pressure of sintering were 650 °C and 500 MPa, respectively. The size of compaction isotropic magnet is 7.5 mm in radius and 15 mm in height. After compaction, the columnar samples were hot deformed into disc-shaped samples with a height reduction of 60 % via SPS in 750 °C. The size of final anisotropic bulk magnet is 12 mm in radius and 6 mm in height. The hot deformed magnet was divided into three parts along radial direction, named "center region" sample, "subcenter region" sample, and "edge region" sample, as shown in Fig. 1(b). The crystal structure and microstructure were characterized by X-ray diffractometry (XRD, XRD-7000) and scanning electron microscopy (SEM, FEI NANO200), respectively. The magnetic properties at room temperature were measured by vibrating sample magnetometry (VSM, Quantum Design Versalab) with a magnetic field up to 30 kOe. The samples with dimensions about 1 mm × 1 mm × 3 mm was cut for VSM measurements. The length direction of the samples was parallel to the applied field during the magnetic measurement and no demagnetization correction was made for all the samples in the magnetic measurements. The electron backscattered diffraction (EBSD) measurements were performed using a high-speed detector (EDAX Hikari camera) incorporated in the scanning electron microscope.

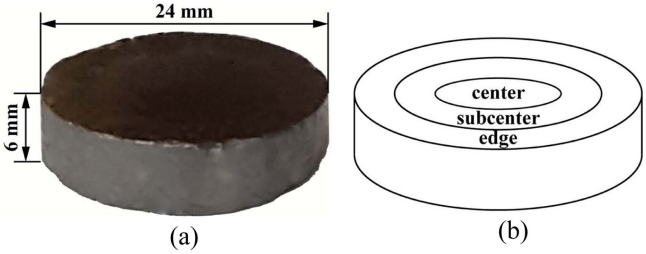

Fig. 1. (Color online) (a) Photograph of the whole hot deformed magnet with dimensions (unit: mm); (b) Schematic illustration for the divisions of the hot deformed magnet.

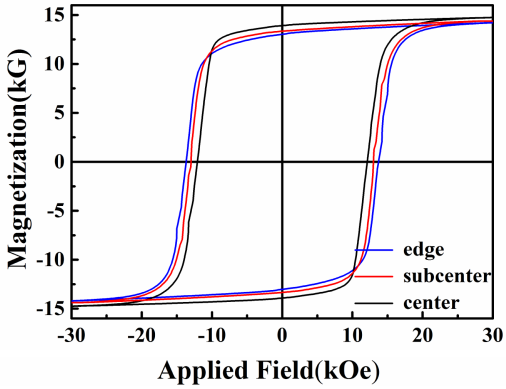

Fig. 2. (Color online) Magnetic hysteresis loops of "center region" sample, "subcenter region" sample and "edge region" sample.

3. Rusults and Discussion

The magnetic hysteresis loops of the three samples are shown in Fig. 2. For all samples, magnetic measurement was carried out along the easy direction, which is parallel to the pressing direction. It is observed that the "center region" sample bear better squareness in the demagnetization curve compared with those of the "subcenter region" and "edge region" samples. Table 1 presents the magnetic properties of the three samples cut from different positions of the hot deformed magnet along radial direction. The high remanence ratios of these three samples indicate that c-axis texture forms throughout the whole sample via hot deformation, leading to strong magnetic anisotropy in the entire magnet. The maximum energy product of 43.72 MGOe is found at the "center" position. Both remanence and maximum energy product decrease monotonically from the "center" to the "edge". The maximum differences in M_r and $(BH)_{max}$ are 0.82 kG and 6.05 MGOe, respectively. While coercivity slightly increases from 12.05 kOe at position "center" to 13.67 kOe at position "edge". These results illustrates that the magnetic performances are heterogeneous at different locations along the radial direction in the bulk magnet.

XRD patterns of the three samples are shown in Fig. 3. The samples were examined with the top surface perpendicular to the radial direction of the disc. All diffraction peaks could be indexed to the standard patterns of $Nd_2Fe_{14}B$. The intensity ratios of (0 0 6) and (1 0 5) peaks which indicate the degree of texture of c-axis crystallographic alignment are 3.13, 1.90 and 0.66 for "center region", "subcenter region" and "edge region" sample, respectively. The XRD patterns of the "edge region" are

Table 1. Magnetic properties of hot deformed Nd–Fe–B samples in different locations.

Sample	M_s (kG)	M_r (kG)	M_r/M_s	H_c (kOe)	$(BH)_{max}$ (MGOe)
center region	14.74	13.95	0.95	12.05	43.72
subcenter region	14.39	13.40	0.93	13.02	40.13
edge region	14.21	13.13	0.92	13.67	37.67

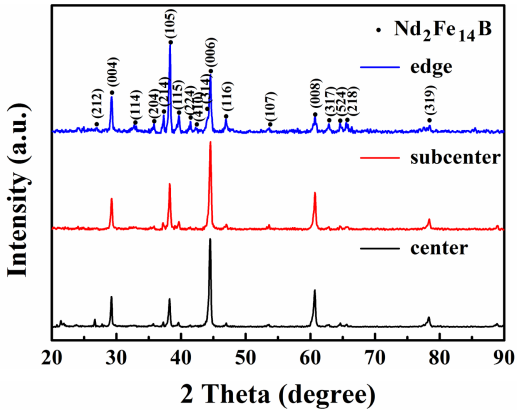

Fig. 3. (Color online) XRD patterns of "center region" sample, "subcenter region" sample and "edge region" sample.

similar to those of the isotropic samples. However, the intensity ratios are obviously increased in the "center region" and "subcenter region". The comparison of intensity ratios suggests that the degree of c-axis crystal alignment is different in the various locations along radial direction [19].

To investigate the origins of radial inhomogeneity of magnetic performance, morphology and microstructures were examined with SEM on the cross-section of hot deformed along radial direction. As shown in Fig. 4(a), (d), and (g), the two distinct zones were noticed in SPS hot deformed Nd–Fe–B samples. The coarse grain zones correspond to the particle boundary area of ribbons and the fine grain zones correspond to the interior of the particles [2]. Meanwhile, it is observed that the microstructure of the fine grain zones consists of small platelet shaped $Nd_2Fe_{14}B$ grains due to the deformation of the grains, as shown in Fig. 4(b), (e), and (h). The grains in the sample at "edge region" have little deformation. This is in agreement with the fact that the crystal texture of this

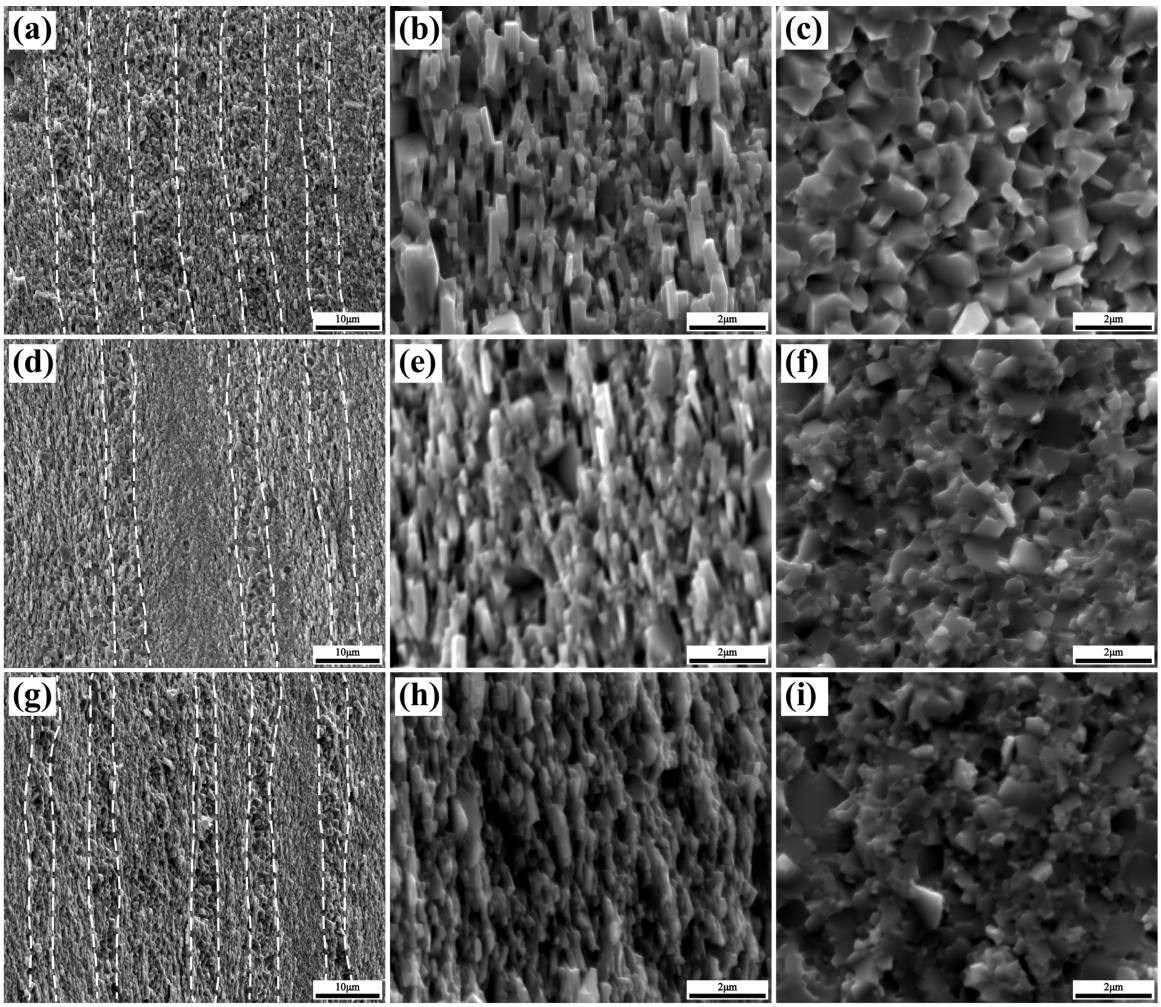

Fig. 4. Microstructure parallel to the pressing direction of hot deformed samples at different locations along radial direction: (a), (b) "center region", (d), (e) "subcenter region"; (g), (h) "edge region". The (c), (f), (i) are the microstructure perpendicular to the pressing direction of three samples, respectively.

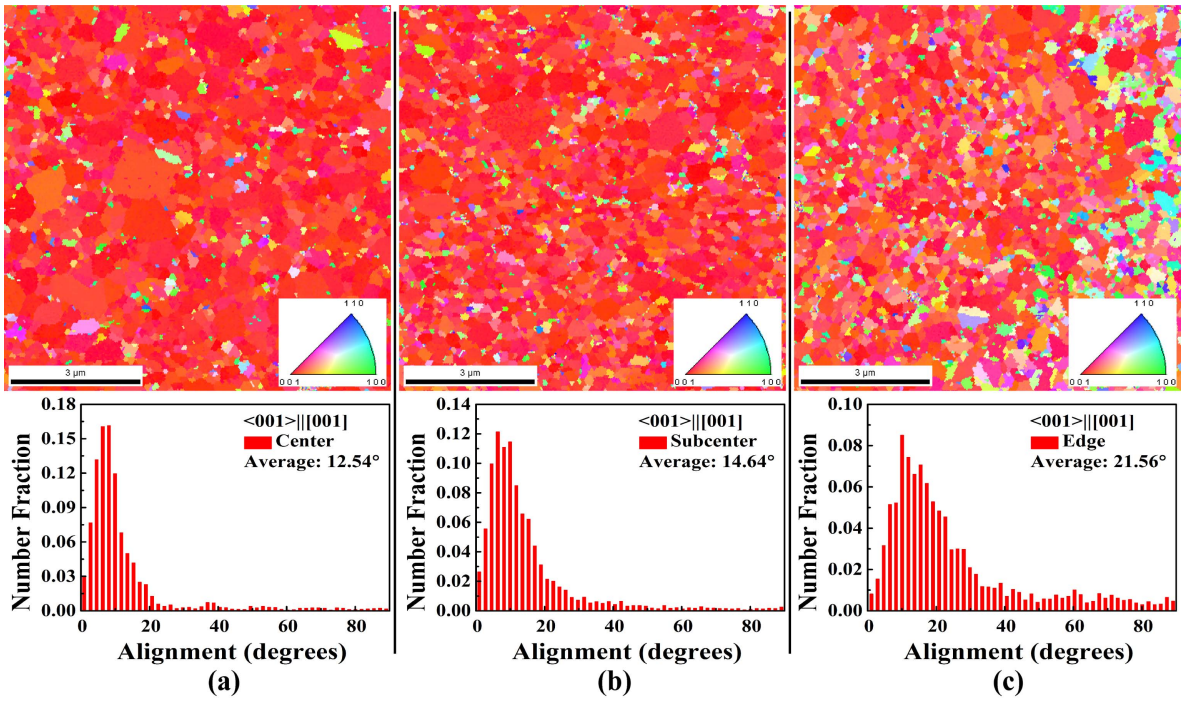

Fig. 5. (Color online) Inverse pole figure quick maps, and the distribution of the individual [00l] deviation from the "ideal orientation" (c-axis parallel to the pressing direction) obtained from the EBSD data of (a) "center region" sample, (b) "subcenter region" sample and (c) "edge region" sample.

sample is similar to that of hot pressed magnet. At "subcenter region", the deformation of $Nd_2Fe_{14}B$ grains is clear. At "center region", $Nd_2Fe_{14}B$ grains exhibit good alignment and the texture of the sample is further enhanced. In addition, the grain microstructures perpendicular to the pressing direction at different locations along radial direction are shown in Fig. 4(c), (f) and (i). The grain size decreases along radial direction from the "center" to the "edge", which can decrease the preferential growth of $Nd_2Fe_{14}B$ grains perpendicular to the pressing direction [14]. This explains why "edge region" magnet has the highest coercivity. The microstructure examined with SEM suggests that grain refining and orientation worsen of $Nd_2Fe_{14}B$ platelets cooperate to result in the improvement of coercivity and deterioration of remanence along radial direction from "center" to "edge" [20].

To further reveal the reasons for the declined M_r and raised H_c along the radial direction from the "center" to the "edge", orientation texture was examined with EBSD over the three samples. Fig. 5 shows inverse pole figure (IPF) quick maps and the distribution of the individual [001] deviation from the "ideal orientation" (c-axis parallel to the pressing direction) obtained from the EBSD data of three samples. The data sets are obtained from the surface perpendicular to the pressure direction. The IPF quick maps are specifically utilized to observe the correlation between the morphological and crystallographic texture. The crystallographic orientation of any $Nd_2Fe_{14}B$ grain can be determined according to the standard IPF orientation legend for a tetragonal system, and the figure indicates the obvious {001} orientation bias of $Nd_2Fe_{14}B$ grains in three samples. Meanwhile, it is easy to discern that "center region" sample have a highest texture. This is in good agreement with the XRD results (Fig. 3). The distribution of the individual [001] deviation from the "ideal orientation" (c-axis parallel to the pressing direction) can also be calculated to measure the intensity of orientation texture. These results show that misorientation angles from ideal orientation of most grains are smaller than 20° in the three samples, which indicates that the analyzed samples are well aligned with [001] oriented parallel to the pressing direction. The average misorientation from ideal orientation of the "center region" is 12.54° while that of "edge region" is 21.56°. Therefore, it is demonstrated that the c-axis texture of the "center region" is better than the "edge region". The results obtained with EBSD are in good agreement with the XRD data.

The quantitative texture analysis is carried out based on the calculation of pole figure (PF) and inverse pole figure (IPF) perpendicular to the pressing direction. Fig. 6 shows the {001} PFs and the IPFs obtained from the EBSD data of the three samples. A significant deviation from ideal

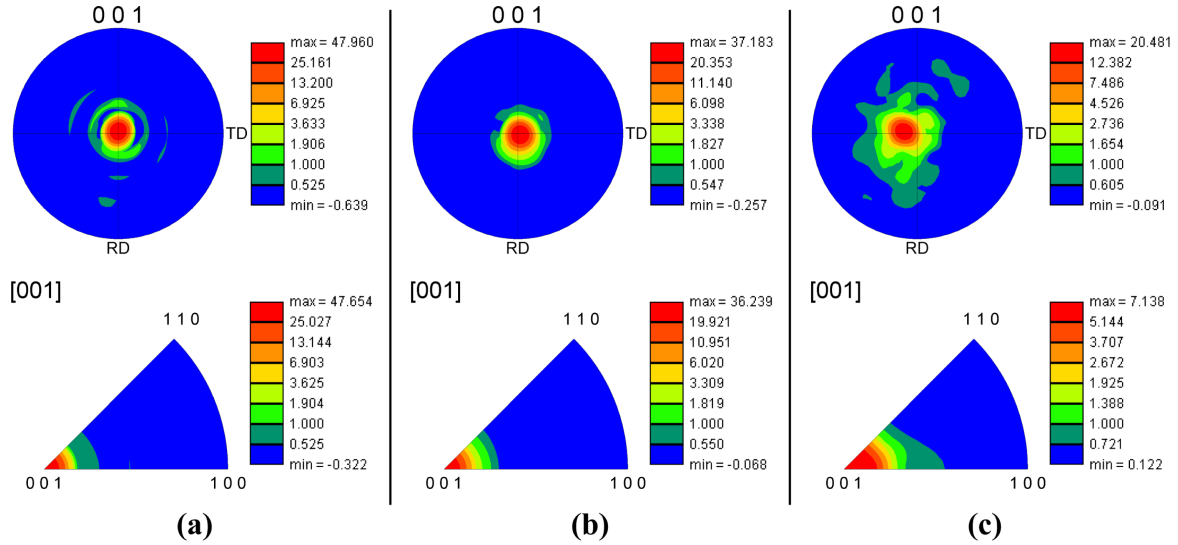

Fig. 6. (Color online) The {001} pole figure (PF) and the inverse pole figure (IPF) perpendicular to the pressing direction in the (a) "center region" sample, (b) "subcenter region" sample and (c) "edge region" sample.

{001} texture is observed for "center region" sample compared with the "edge region" sample, indicating a better {001} orientation texture in the "center region" sample. This can also be concluded from the quantitative expression in terms of the intensity of the central pole. The maximum intensities of the "center region" sample is the highest which is approximately 47.96 Multiple of a Random Distribution (MRD) in PF and 47.65 MRD in IPF, while those of the "edge region" sample are the lowest. The lower MRD values also suggest a weaker texture in the sample.

Therefore, the degree of c-axis crystal alignment of $Nd_2Fe_{14}B$ platelets was confirmed to decrease monotonically from the "center" to the "edge", which result in the decrease of both remanence and maximum energy product. Meanwhile, the width of $Nd_2Fe_{14}B$ platelets decrease from the "center" to the "edge" as shown in Fig. 4(c), (f) and (i). The larger ratio of width to thickness would enhance the irregular degree of grain, which possibly increases the stray field acting on the grains in the "center region". In addition, better c-axis crystal alignment would also enhance the stray field in the sample of "center region". These two effects cooperate to result in the improvement of coercivity from "center" to "edge" [2].

4. Conclusion

In summary, the anisotropic Nd–Fe–B magnet was prepared by hot deformation methods. The hot deformed permanent magnets exhibit inhomogeneous magnetic performance in radial direction along which the maximum energy product increases obviously from the "edge" to the "center", while coercivity decreases slightly. The XRD, SEM and EBSD characterizations suggest that the enhanced c-axis texture in "center region" results in the stronger magnetic anisotropy and increased maximum energy product. Simultaneously, the grain size decreases from "center" to "edge", which leads to the coercivity increasing.

Acknowledgment

This work was supported by the National Natural Science Foundation of China (51401001, 51701109 and 51331003) and International S&T Cooperation Program of China (2015DFG52020).

References

[1] T. Wang, M. Yue, Y. Q. Li, M. Tokita, Q. Wu, D. T. Zhang, and J. X. Zhang, IEEE Magn. Lett. **6**, 5500304 (2015).
[2] Y. H. Hou, Y. L. Huang, Z. W. Liu, D. C. Zeng, S. C. Ma, and Z. C. Zhong, Mater. Sci. Eng.: B **178**, 990 (2013).
[3] S. Liu, N. H. Kang, L. Feng, S. H. Lee, J. H. Yu, and J. G. Lee, IEEE Trans. Magn. **51**, 20130204 (2015).
[4] H. L. Li, L. Lou, F. C. Hou, D. F. Guo, W. Li, X. H. Li, D. V. Gunderov, K. Sato, and X. Y. Zhang, Appl. Phys. Lett. **103**, 142406 (2013).
[5] Y. G. Liu, L. Xu, Q. F. Wang, W. Li, and X. Y. Zhang, Appl. Phys. Lett. **94**, 172502 (2009).
[6] G. C. Hadjipanayis, J. Magn. Magn. Mater. **200**, 373 (1999).
[7] A. H. Li, W. Li, B. Lai, H. J. Wang, M. G. Zhu, and W.

Pan, J. Appl. Phys. **107**, 09A725 (2010).
[8] W. Z. Yin, R. J. Chen, X. Tang, M. Lin, D. Lee, and A. Yan, J. Appl. Phys. **111**, 07A727 (2012).
[9] M. Yue, J. Zhang, M. Tian, and X. B. Liu, J. Appl. Phys. **99**, 08B502 (2006).
[10] H. L. Li, H. X. Li, D. F. Guo, L. Lou, W. Li, and X. Y. Zhang, Nano Lett. **16**, 5631 (2016).
[11] X. L. Li, L. Lou, W. P. Song, G. W. Huang, F. C. Hou, Q. Zhang, H. T. Zhang, J. W. Xiao, B. Wen, and X. Y. Zhang, Adv. Mater. **29**, 1606430 (2017).
[12] X. L. Li, L. Lou, W. P. Song, Q. Zhang, G. W. Huang, Y. X. Hua, H. T. Zhang, J. W. Xiao, B. Wen, and X. Y. Zhang, Nano Lett. **17**, 2985 (2017).
[13] W. Q. Liu, Z. Z. Cui, X. F. Yi, M. Yue, Y. B. Jiang, D. T. Zhang, J. X. Zhang, and X. B. Liu, J. Appl. Phys. **107**, 09A719 (2010).
[14] Z. W. Liu, H. Y. Huang, X. X. Gao, H. Y. Yu, X. C. Zhong, J. Zhu, and D. C. Zeng, J. Phys. D: Appl. Phys. **44**, 025003 (2011).
[15] S. J. Lillywhite, A. J. Williams, B. E. Davies, and I. R. Harris, J. Microsc. **205**, 270 (2002).
[16] X. C. Xu, H. G. Zhang, T. Wang, Y. Q. Li, D. T. Zhang, and M. Yue, J. Alloys Compd. **699**, 262 (2017).
[17] C. G. Hauegen, F. R. Freitas Da Silva, F. A. Sampaio Da Silva, J. F. C. Lins, and M. F. De Campos, Advanced Powder Technology VIII, **727-728**, 135 (2012).
[18] M. F. De Campos, T. Yonamine, M. Fukuhara, R. Machado, S. A. Romero, F. J. G. Landgraf, D. Rodrigues, and F. P. Missell, J. Appl. Phys. **101**, 09K516 (2007).
[19] D. T. Zhang, X. K. Yuan, M. Yue, Q. Ma, J. Zhu, and J. X. Zhang, RSC Advances **5**, 90976 (2015).
[20] W. Z. Yin, R. J. Chen, X. Tang, X. Tang, D. Lee, and A. Yan, IEEE Trans. Magn. **50**, 2100704 (2014).